Progressive damage analysis of composite structures using higher-order layer-wise elements

Progressive Damage Analysis of Composite Structures Using Higher-Order Layer-Wise Elements

M. H. Nagaraj[1], J. Reiner[2], R. Vaziri[3], E. Carrera*[1], and M. Petrolo[1]

[1]MUL[2] Group, Department of Mechanical and Aerospace Engineering, Politecnico di Torino, Corso Duca degli Abruzzi 24, 10129 Torino, Italy
[2]School of Engineering, Deakin University, Geelong, Australia
[3]Composites Research Network, The University of British Columbia, Vancouver, Canada

Submitted to

Composites Part B: Engineering

Author for correspondence:
E. Carrera, Professor of Aerospace Structures and Aeroelasticity,
MUL[2] Group, Department of Mechanical and Aerospace Engineering,
Politecnico di Torino,
Corso Duca degli Abruzzi 24,
10129 Torino, Italy,
tel: +39 011 090 6836,
fax: +39 011 090 6899,
e-mail: erasmo.carrera@polito.it

Abstract

The objective of the current work is the development of a numerical framework for the simulation of damage in composite structures using explicit time integration. The progressive damage is described using a Continuum Damage Mechanics (CDM) based material model, CODAM2, in which the damage initiation and progression are modelled using Hashin's failure criteria and crack-band theory, respectively. The structural modelling uses higher-order theories based on the Carrera Unified Formulation (CUF). The current work considers 2D-CUF models where Lagrange polynomials are used to represent the displacement field through the thickness of each ply, resulting in a layer-wise element model. Numerical assessments are performed on coupon-level specimens, and the results are shown to be in good agreement with reference numerical predictions and experimental data, thus verifying the current implementation for progressive tensile damage. The capability of the proposed framework in increasing the polynomial expansion order through the ply thickness, and its influence on the global behaviour of the structure in the damaged state, is demonstrated. The advantages of using higher-order structural models in achieving significant improvements in computational efficiency are highlighted.

Keywords: CODAM2, CUF, explicit damage analysis, higher-order structural modelling

1 Introduction

Fibre reinforced composites have become very popular as an engineering material system in recent decades due to their desirable properties. This is especially true in the aerospace industry due to the high specific stiffness and strength of such materials. However, wide-spread adoption of composites has still not been achieved, due to uncertainties regarding their non-linear behaviour. Laminated composites typically exhibit extremely complex failure modes, and the accurate modelling of such mechanisms is a challenging task. Nevertheless, several attempts have been made by researchers to develop damage models for composite materials [1, 2].

Computational damage models for composite structures can be generalised into two broad categories. The first approach, based on discrete modelling, involves the explicit geometrical representation of cracks within the structure. Such a technique results in a physically realistic description of the damage mechanisms and their interactions, but at the expense of greatly increased computational effort. The discrete modelling approach typically makes use of interface elements, based on cohesive zone modelling, to simulate both matrix cracks within the ply as well as delamination between the plies [3–7]. Other discrete modelling techniques involve the eXtended-Finite Element Method (XFEM) where enriched kinematics are used to describe the displacement discontinuity across the crack [8, 9], and the floating node method [10, 11].

An alternative approach to discrete damage modelling is based on the concept of continuum damage mechanics (CDM), where the continuity of the displacement field in the finite element mesh is maintained. In contrast to discrete damage modelling, the individual cracks within the composite material are smeared out in CDM approaches, and replaced with damage parameters in the constitutive relationship to describe the influence of such cracks on the global structural behaviour. CDM techniques are popular due to their ease of implementation and relatively low computational cost. However, they generally exhibit a strong mesh dependency, which is reduced by scaling the fracture energy using a characteristic element length, as described by the crack-band theory [12]. Some early works on continuum damage modelling of composite laminates include the works of Ladaveze et al. [13] and Matzenmiller et al. [14]. Some recent works based on continuum damage modelling include the investigation of size effects in notched composites [15], impact analysis of composite plates [16], and progressive damage analysis of composite pressure vessels [17]. A popular approach for composite damage modelling is a combination of CDM to describe intralaminar damage within the ply, and discrete approaches such as the cohesive zone method to model delamination. Such an approach constitutes a good compromise between computational effort and accuracy. Some examples of the application of the combined technique are the failure analysis of open-hole tension laminates [18], damage and delamination analysis of hybrid composite joints [19], and impact analysis of composites [20, 21].

The current work considers a purely continuum damage approach, where intralaminar damage within the ply is described using the COmposite DAMage (CODAM) model. The CODAM model was originally developed as a sub-laminate based continuum damage model [22], and applied to the simulation of braided composite tubes under axial crushing [23]. CODAM has also been combined with an adaptive local cohesive zone method for the efficient analysis of composites under axial crushing and transverse impact loading [24]. The second-generation damage model, termed CODAM2, is a strain-based damage formulation at the ply level which can be applied to the macro and meso-scale [25–27]. This version is implemented as a built-in material model (MAT219) in the explicit finite element software LS-DYNA. The latest extension of CODAM2 includes a stress-based criterion for damage initiation and a coupling between matrix damage and delamination [28], and is the version that has been implemented in the current work. The structural modelling is performed using higher-order structural theories based on the Carrera Unified Formulation (CUF) [29], which is a generalised framework to develop refined 1D and 2D models where the kinematic field is enriched via the use of cross-section and thickness expansion functions, respectively. Such an approach results in 3D-like accuracy of the solution while avoiding the computational costs associated with standard 3D-FEA. The current work aims to extend the capabilities of CUF as a virtual testing framework. Previous works in CUF include the nonlinear analysis of thin-walled structures [30, 31], micromechanical progressive failure analysis of composites [32], and multi-scale analysis [33, 34]. This paper is divided into the following parts - Section 2 describes the development of 2D structural theories in CUF and Section 3 provides a brief overview of the CODAM2 intralaminar damage model. Some numerical test cases are given in Section 4, and the results are discussed in Section 5. The conclusions of the present work are highlighted in Section 6.

2 Structural theories and FE formulation

2.1 Carrera Unified Formulation

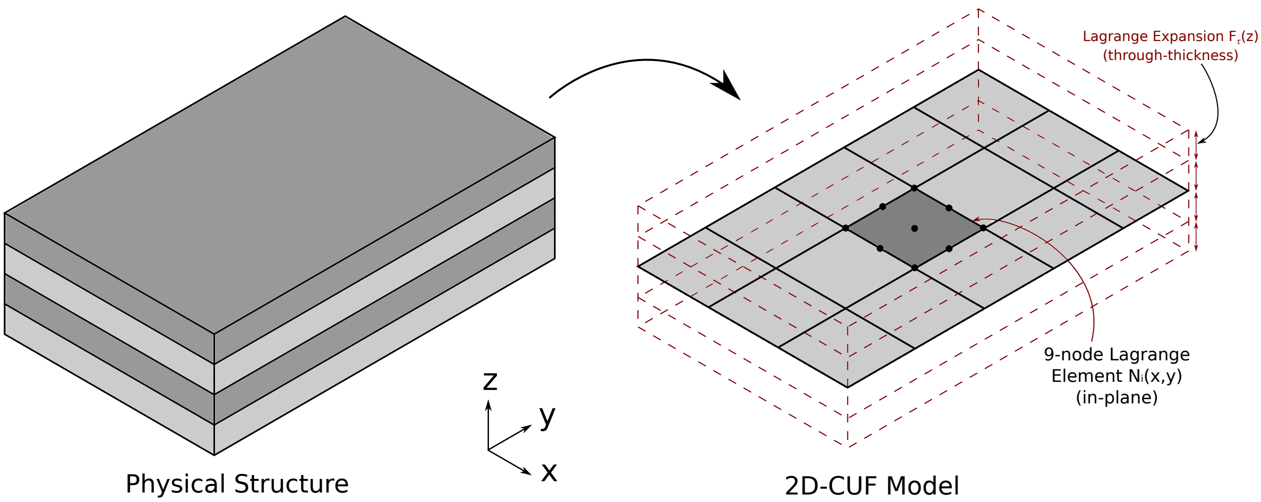

Figure 1: Layer-wise modelling of composite laminates in CUF. This approach uses 9-node second-order quadrilateral (Q9) elements to model the in-plane geometry, while Lagrange polynomial expansion functions are used for the explicit description of individual plies.

Consider a 3D physical structure which consists of a laminated plate, as shown in Fig. 1. The 2D-CUF model is also schematically shown in the figure, with the in-plane geometry of the structure oriented along the x-y plane, and the thickness described along the z-axis. The displacement field is defined in CUF as

$$
\begin{aligned}
u(x, y, z) &= F_0(z)u_0(x, y) + F_1(z)u_1(x, y) + \ldots + F_N(z)u_N(x, y) \\
v(x, y, z) &= F_0(z)v_0(x, y) + F_1(z)v_1(x, y) + \ldots + F_N(z)v_N(x, y) \\
w(x, y, z) &= F_0(z)w_0(x, y) + F_1(z)w_1(x, y) + \ldots + F_N(z)w_N(x, y)
\end{aligned}
\tag{1}
$$

Considering a layer-wise (LW) modelling approach, the displacements can be written in a compact form as

$$
\mathbf{u}^k(x, y, \zeta_k) = F_\tau^k(\zeta_k)\mathbf{u}_\tau(x, y), \tau = 0, 1, \ldots M \tag{2}
$$

where k is the ply index of the laminated plate, the expansion function $F_\tau(\zeta_k)$ describes the kinematics through the thickness of ply k with the thickness domain $\zeta_k \in [-1, 1]$, and $\mathbf{u}_\tau(x, y)$ are the generalised displacements. The number of terms in the expansion function is denoted by M. The choice of the expansion, F_τ, and the number of terms, M, determines the structural theory used in the analysis. The current work considers Lagrange interpolation polynomials to define the expansion through the thickness. In CUF terminology, such a choice is termed the Lagrange-Expansion (LE) class. The current work considers first-order linear expansions (LE1), second-order quadratic expansions (LE2), and third-order cubic expansions (LE3). For the case of LW modelling with Lagrange expansions, the displacements at the layer interfaces obey the following compatibility condition

$$
u_{top}^k = u_{bottom}^{k+1}, \; k = 1, N_{ply} - 1 \tag{3}
$$

The use of thickness functions from the LE class results in purely displacement degrees of freedom, and eliminates rotations. Further details on the use of Lagrange polynomials as a class of expansion function in 1D-CUF models may be found in [35], while an overview of 2D plate modelling in CUF can be found in [36].

2.2 Finite Element Formulation

The stress and strain tensors are defined in vector notation as

$$
\begin{aligned}
\boldsymbol{\sigma} &= \{\sigma_{xx}, \sigma_{yy}, \sigma_{zz}, \sigma_{xy}, \sigma_{xz}, \sigma_{yz}\} \\
\boldsymbol{\varepsilon} &= \{\varepsilon_{xx}, \varepsilon_{yy}, \varepsilon_{zz}, \varepsilon_{xy}, \varepsilon_{xz}, \varepsilon_{yz}\}
\end{aligned}
\tag{4}
$$

The linear strain-displacement relation is then expressed as

$$
\boldsymbol{\varepsilon} = \mathbf{D}\mathbf{u} \tag{5}
$$

where the differential operator, $\mathbf{D}$, is

$$\mathbf{D} = \begin{bmatrix} \frac{\partial}{\partial x} & 0 & 0 \\ 0 & \frac{\partial}{\partial y} & 0 \\ 0 & 0 & \frac{\partial}{\partial z} \\ \frac{\partial}{\partial y} & \frac{\partial}{\partial x} & 0 \\ \frac{\partial}{\partial z} & 0 & \frac{\partial}{\partial x} \\ 0 & \frac{\partial}{\partial z} & \frac{\partial}{\partial y} \end{bmatrix}$$

The constitutive relation is given by

$$\boldsymbol{\sigma} = \mathbf{C}^{sec} \boldsymbol{\varepsilon} \tag{6}$$

where $\mathbf{C}^{sec}$ is the secant material stiffness matrix, obtained from the CODAM2 damage model as described in Section 3. The damaged stress state is then represented by $\boldsymbol{\sigma}$. The in-plane geometry is discretised with 9-node quadrilateral finite elements (Q9), using nodal interpolation functions $N_i(x, y)$, leading to the following 3D form of the displacement field

$$\mathbf{u}(x, y, z) = N_i(x, y) F_\tau(z) \mathbf{u}_{\tau i} \tag{7}$$

2.3 Explicit time integration

The semi-discrete balance of momentum is given by

$$\mathbf{M}\ddot{\mathbf{a}}^{t+\Delta t} = \mathbf{f}_{ext}^{t+\Delta t} - \mathbf{f}_{int}^{t+\Delta t} \tag{8}$$

where $\mathbf{M}$ is the mass matrix and $\mathbf{f}_{ext}$ and $\mathbf{f}_{int}$ are the external and internal force vectors, respectively. The nonlinear dynamic problem is solved explicitly using the central difference scheme, whose formulation can be found, for instance, in [37]. The version of the central difference scheme employed in the current work approximates the velocity at the mid-interval such that

$$\dot{\mathbf{u}}^{t+\frac{1}{2}\Delta t} = \frac{\mathbf{u}^{t+\Delta t} - \mathbf{u}^t}{\Delta t} \tag{9}$$

where $\mathbf{u}$ and $\dot{\mathbf{u}}$ are the displacement and velocity vectors, respectively. Equation 9 is re-written to obtain an expression for the displacement update

$$\mathbf{u}^{t+\Delta t} = \mathbf{u}^t + \Delta t \; \dot{\mathbf{u}}^{t+\frac{1}{2}\Delta t} \tag{10}$$

The updated displacements are used to calculate the new strain and stress states, leading to the computation of $\mathbf{f}_{int}^{t+\Delta t}$. The updated acceleration is directly computed from Eq. 8 as

$$\ddot{\mathbf{u}}^{t+\Delta t} = \mathbf{M}^{-1}\{\mathbf{f}_{ext}^{t+\Delta t} - \mathbf{f}_{int}^{t+\Delta t}\} \tag{11}$$

The mid-interval velocity for the next cycle, required for Eq. 10, is computed from the acceleration as

$$\dot{\mathbf{u}}^{t+\frac{3}{2}\Delta t} = \dot{\mathbf{u}}^{t+\frac{1}{2}\Delta t} + \Delta t\ \ddot{\mathbf{u}}^{t+\Delta t} \tag{12}$$

At the start of the solution ($t = 0$), the mid-interval velocity $\dot{\mathbf{u}}^{\frac{1}{2}\Delta t}$ is required to solve Eq. 10. This term is determined by the following assumption

$$\dot{\mathbf{u}}^{\frac{1}{2}\Delta t} = \dot{\mathbf{u}}^{0} + \frac{1}{2}\Delta t\ \ddot{\mathbf{u}}^{0} \tag{13}$$

where the initial velocity, $\dot{\mathbf{u}}^0$, and the initial acceleration, $\ddot{\mathbf{u}}^0$, are based on the initial conditions of the system. Finally, a lumped mass matrix is considered in Eq. 11, which results in computationally inexpensive vector multiplication. The row summing technique is utilised to obtain the lumped mass matrix. The algorithm for the central difference scheme with mid-interval velocities has been summarised in Table 1.

Table 1: Algorithm for the central difference time integration scheme [37]

Initialise $\mathbf{u}^0$ and $\dot{\mathbf{u}}^0$
Compute the lumped mass matrix $\mathbf{M}$
Compute initial mid-interval velocity: $\dot{\mathbf{u}}^{\frac{1}{2}\Delta t} = \dot{\mathbf{u}}^{0} + \frac{1}{2}\Delta t\ \ddot{\mathbf{u}}^{0}$

For each time increment:
1. Compute new displacements: $\mathbf{u}^{t+\Delta t} = \mathbf{u}^{t} + \Delta t\ \dot{\mathbf{u}}^{t+\frac{1}{2}\Delta t}$
2. Compute displacement increment: $\Delta\mathbf{u} = \mathbf{u}^{t+\Delta t} - \mathbf{u}^{t}$
3. For each integration point:
→ Compute updated strains: $\boldsymbol{\varepsilon}^{t+1} = \boldsymbol{\varepsilon}^{t} + \mathbf{B}\Delta\mathbf{u}$
→ Compute updated stress: $\boldsymbol{\sigma}^{t+1} = \mathbf{C}^{sec}\boldsymbol{\varepsilon}^{t+1}$
4. Compute internal force vector: $\mathbf{f}_{int}^{t+\Delta t} = \int_V \mathbf{B}^T\boldsymbol{\sigma}^{t+\Delta t}\ dV$
5. Compute new accelerations: $\ddot{\mathbf{u}}^{t+\Delta t} = \mathbf{M}^{-1}\{\mathbf{f}_{ext}^{t+\Delta t} - \mathbf{f}_{int}^{t+\Delta t}\}$
6. Compute new mid-interval velocities: $\dot{\mathbf{u}}^{t+\frac{3}{2}\Delta t} = \dot{\mathbf{u}}^{t+\frac{1}{2}\Delta t} + \Delta t\ \ddot{\mathbf{u}}^{t+\Delta t}$

The critical time step for the analysis is determined by computing the highest frequency of the system, ω_{max}, and using the following expression

$$\Delta t_{critical} = \frac{2}{\omega_{max}} \tag{14}$$

3 CODAM2 intralaminar damage model

The ply-based form of the CODAM2 stress-based damage model has been considered in the current work. Damage initiation occurs when the damage initiation function $F_\alpha \geq 1$, in the fibre ($\alpha = 1$) and transverse ($\alpha = 2$) direction. Damage initiation along the longitudinal direction, i.e. fibre damage, is described by F_1, which is a maximum stress criterion given by

$$F_1 = \frac{\sigma_{11}}{X_T} \tag{15}$$

where X_T is the fibre tensile strength. Stress and strain components with the subscripts $\{11, 22, 12\}$ indicate the fields have been rotated into the material reference system. Similarly, damage initiation along the transverse direction, i.e. matrix damage, is described by Hashin's quadratic failure criterion [38] as

$$F_2 = \left(\frac{\sigma_{22}}{Y_T}\right)^2 + \left(\frac{\tau_{12}}{S_L}\right)^2 \tag{16}$$

where Y_T and S_L are the transverse tensile and in-plane shear strength, respectively. The damage progression criteria requires the equivalent strain measures ε_1^{eq} and ε_2^{eq} in the longitudinal and transverse directions respectively, as damage drivers, and are defined as

$$\varepsilon_1^{eq} = |\varepsilon_{11}| \tag{17}$$

$$\varepsilon_2^{eq} = \sqrt{(\gamma_{12}^e)^2 + (\varepsilon_{22})^2} \tag{18}$$

where γ_{12}^e refers to the elastic component of the shear strain. The corresponding equivalent stress measures are

$$\sigma_1^{eq} = \sigma_{11} \tag{19}$$

$$\sigma_2^{eq} = \frac{\tau_{12}\gamma_{12}^e + \sigma_{22}\varepsilon_{22}}{\sqrt{(\gamma_{12}^e)^2 + (\varepsilon_{22})^2}} \tag{20}$$

The strains at damage initiation are given by

$$\varepsilon_\alpha^i = \varepsilon_\alpha^{eq}|_{F_\alpha=1}, \qquad \alpha = 1, 2 \tag{21}$$

Subsequently, the strains at damage saturation are defined as

$$\varepsilon_1^s = \frac{2g_1^f}{X_T} \quad and \quad \varepsilon_2^s = \frac{2g_2^f}{T} \tag{22}$$

where g_α^f is the fracture energy density, and $T = \sigma_2^{eq}|_{F_2=1}$ is the peak value of the equivalent transverse stress σ_2^{eq}. The crack-band approach [12] is used to reduce mesh dependency by scaling the experimentally determined fracture energy G_α^f, using a characteristic length parameter of the element, as follows

$$g_\alpha^f = \frac{G_\alpha^f}{l^*}, \quad \alpha = 1, 2 \tag{23}$$

where l^* is the characteristic element length. The current work considers $l^* = (V_{GP})^{\frac{1}{3}}$, where V_{GP} is the Gauss point volume of the given element. In contrast to [26], the local form of the CODAM2 model is implemented herein, such that Eq. 23 is applicable for both longitudinal and transverse directions. The damage parameters ω_α, used to evaluate damage progression, are defined as

$$\omega_\alpha = \left(\frac{< \varepsilon_\alpha^{eq} - \varepsilon_\alpha^i >}{\varepsilon_\alpha^s - \varepsilon_\alpha^i} \right) \left(\frac{\varepsilon_\alpha^s}{\varepsilon_\alpha^{eq}} \right), \quad \alpha = 1, 2 \tag{24}$$

where $< \cdot >$ denotes the Macaulay bracket. Using the damage variables, the 3D form of the secant stiffness matrix in the damaged state [28] is written as

$$\mathbf{C}^{dam} = \frac{1}{\Delta} \begin{bmatrix} (1 - R_2\nu_{23}\nu_{32})R_1E_1 & (\nu_{21} + \nu_{23}\nu_{31})R_1R_2E_1 & (\nu_{31} + R_2\nu_{21}\nu_{32})R_1E_1 & 0 & 0 & 0 \\ & (1 - R_1\nu_{31}\nu_{13})R_2E_2 & (\nu_{32} + R_1\nu_{31}\nu_{12})R_2E_2 & 0 & 0 & 0 \\ & & (1 - R_1R_2\nu_{21}\nu_{12})E_3 & 0 & 0 & 0 \\ & & & \Delta R_1R_2G_{12} & 0 & 0 \\ & sym. & & & \Delta G_{23} & 0 \\ & & & & & \Delta G_{13} \end{bmatrix} \tag{25}$$

where $\Delta = 1 - R_2\nu_{23}\nu_{32} - R_1R_2\nu_{12}\nu_{21} - 2R_1R_2\nu_{31}\nu_{12}\nu_{23} - R_1\nu_{31}\nu_{13}$ and R_α denotes the stiffness reduction factor, given by

$$R_\alpha = (1 - \omega_\alpha), \quad \alpha = 1, 2 \tag{26}$$

Finally, the stress state is computed as

$$\boldsymbol{\sigma} = \mathbf{C}^{dam}\boldsymbol{\varepsilon} \tag{27}$$

4 Numerical Examples

The current section consists of a series of numerical assessments which serve as validation cases for the proposed modelling approach. The material system used in each case is IM7/8552 carbon fibre reinforced polymer (CFRP), and its properties are given in Table 2.

Table 2: Material properties of the IM7/8552 CFRP material system [39]

Material	E_1 [GPa]	E_2 [GPa]	E_3 [GPa]	G_{12} [GPa]	G_{13} [GPa]	G_{23} [GPa]	ν_{12}	ν_{13}	ν_{23}
IM7/8552 CFRP	165.0	9.0	9.0	5.6	5.6	2.8	0.34	0.34	0.5
		X_T [MPa]	Y_T [MPa]	S_L [MPa]	G_1^f $[kJ/m^2]$ [40]	G_2^f $[kJ/m^2]$ [28]			
		2560.0	73.0	90.0	120.0	2.6			

4.1 Single element tests

The first set of numerical assessments consists of single element tests under uni-axial strain conditions, which are a convenient way of verifying the implementation of the damage model, since the different failure modes can be independently evaluated. In each case, the in-plane geometry is modelled using a 4-node quadrilateral element (Q4), with the ply thickness modelled using a linear Lagrange polynomial (LE1). The first test involves a single element under longitudinal tension, which results in a fibre failure mode. The stress-strain curve for this case is shown in Fig. 2a. Next, the single element is subjected to transverse tension, resulting in a matrix failure mode. The stress-strain curve for this case has been plotted in Fig. 2b. The final assessment is the tensile loading of a single element consisting of a quasi-isotropic laminate with a $[90/45/0/-45]_{2s}$ layup. For this case, the predicted stress-strain curve is shown in Fig. 3. The results are compared to the CODAM2 reference model [26], implemented as a user-defined subroutine in LS-DYNA.

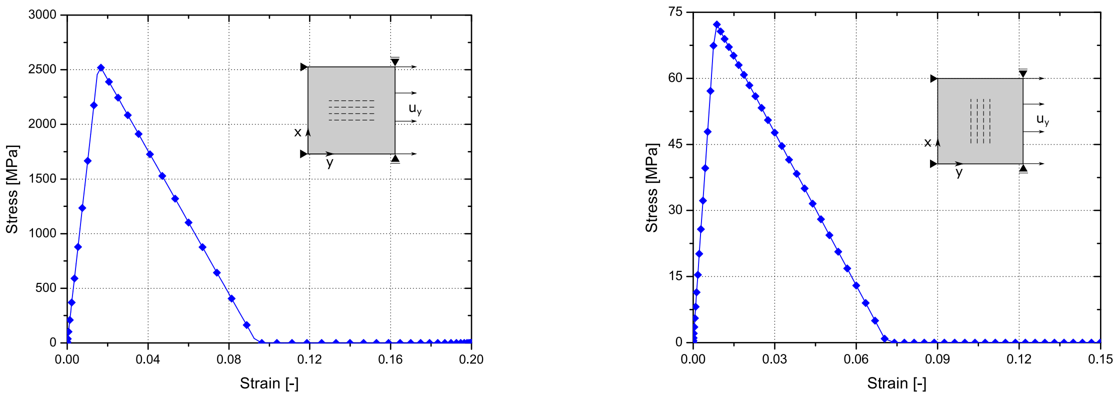

(a) Longitudinal loading (fibre) **(b)** Transverse loading (matrix)

Figure 2: Stress-strain curve of a single element loaded in tension under uni-axial strain conditions. (a) Element loaded in the longitudinal (fibre) direction, and (b) Element loaded in the transverse (matrix dominated) direction

The following observations are made

1. The stress-strain curves shown in Fig. 2 follow the bilinear degradation law described by the CODAM2 damage model, and the peak stresses predicted by the CUF models under longitudinal and transverse tension are equal to the fibre and matrix material strengths, respectively, i.e., the analysis output is consistent with the input material strength values.

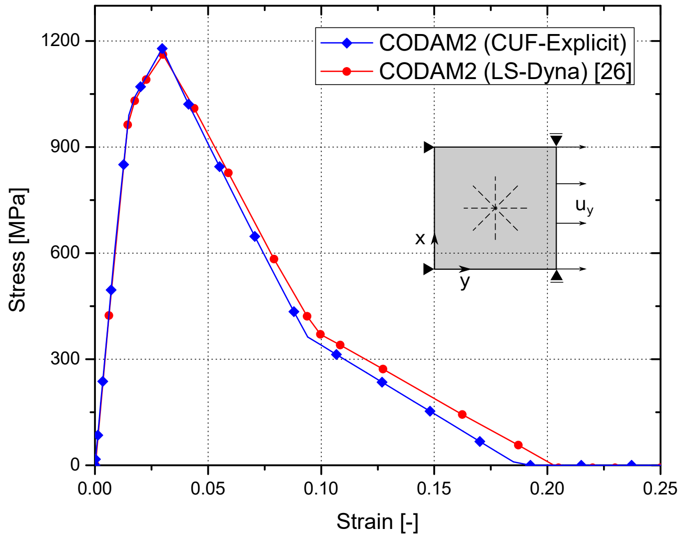

Figure 3: Stress-strain response of the single element $[90/45/0/-45]_{2s}$ IM7/8552 CFRP quasi-isotropic laminate in tension under uniaxial strain condition

2. The results of the single element laminate obtained by the present implementation is in good agreement with reference numerical results, as shown in Fig. 3.

   The above observations verify the implementation of the CODAM2 damage model in CUF-Explicit.

4.2 Centre-notched tension specimen

The current example concerns the analysis of a centre-notched tensile (CNT) specimen. The structure is shown schematically in Fig. 4, and the ply stacking sequence is $[45/90/-45/0]_{4s}$. The coupon is constrained at one end, and a displacement u_y is applied to the opposite end. Various scales of the coupon have been numerically analysed, in order to demonstrate the capability of the current framework in predicting size-effects in composite structures. The various scales used, and their dimensions, are listed in Table 3. The current example is based on the works of [26], which provides reference numerical results based on the LS-DYNA implementation of the CODAM2 model. In addition, reference numerical results are also obtained from the *ABQ_DLR* model, which is a Ladavèze-based damage model, implemented as a user-material (VUMAT) in ABAQUS/Explicit [26]. The peak strengths predicted in the current work have also been compared with experimentally obtained data [41]. The mesh used in the CUF-Explicit analyses (scales 1-16) consist of 132 quadratic (second-order, Q9) elements within the plane, while the scale-24 analysis consists of a 244 Q9 mesh. The mesh-size in the fracture process zone is approximately 4 mm $\times$ 0.5 mm for the case of the scale-8 mesh. All the CUF models use a linear (first-order, LE1) Lagrange polynomial expansion to explicitly model each ply. In the case of the scale-8 specimen, three models are considered, where the plies are modelled using a linear (first-order, LE1), quadratic (second-order, LE2) and cubic (third-order, LE3) expansion, respectively, as described in Section 2.1.

Figure 5 shows the stress-strain curve for the scale-8 CNT specimen, as obtained from the various modelling

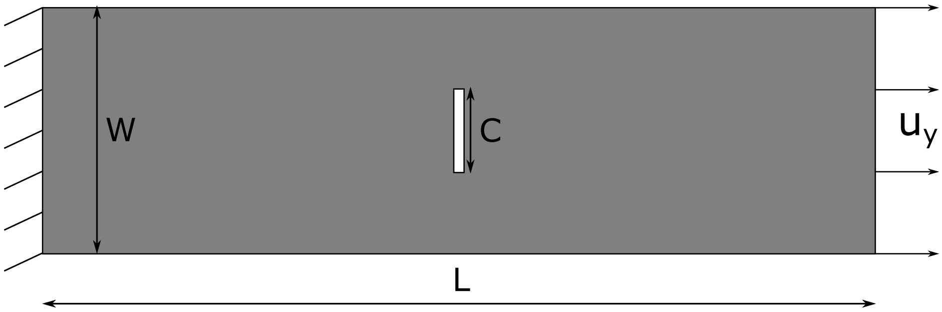

Figure 4: Schematic representation of the centre-notched tensile specimen geometry and applied boundary conditions

Table 3: Dimensions of the various scales of the CNT specimen

Scale	Notch Length C [mm]	Specimen Width [mm]	Specimen Length [mm]
1	3.2	15.9	63.5
2	6.4	31.8	127.0
4	12.7	63.5	254.0
8	25.4	127.0	508.0
16	50.8	254.0	508.0
24*	76.2	381.0	1016.0

* Virtual test sample

approaches. The peak stress (strength) for the various scales have been plotted in Fig. 6. Comparisons have been made with experimental and reference numerical results in both cases. The influence of the structural dimensions on the overall computational cost of the analysis has been investigated, in terms of the degrees of freedom (DOF) required, as shown in Fig. 7a, and normalised computational time, as shown in Fig. 7b. The computational times have been normalised for each model type using the computational time required for the analysis of the scale-1 specimen.

Based on the results, the following comments can be made

1. From Fig. 5, a brittle behaviour of the specimen can be observed, with a linear elastic increase of the stress until the maximum value is reached, followed by abrupt loss of stiffness leading to failure. The response predicted by the current approach is in good agreement with reference numerical and experimental results.

2. The influence of the ply thickness expansion order, in the case of CUF models, can be seen in Fig. 5. The use of LE1 expansions through the ply results in a lower peak strength compared to LE2, while there is no difference between LE2 and LE3 expansions.

3. A clear size-effect can be observed in Fig. 6, based on the peak strengths, through the scales of the CNT specimen. The predictions of the current framework are in good agreement with reference numerical and experimental results.

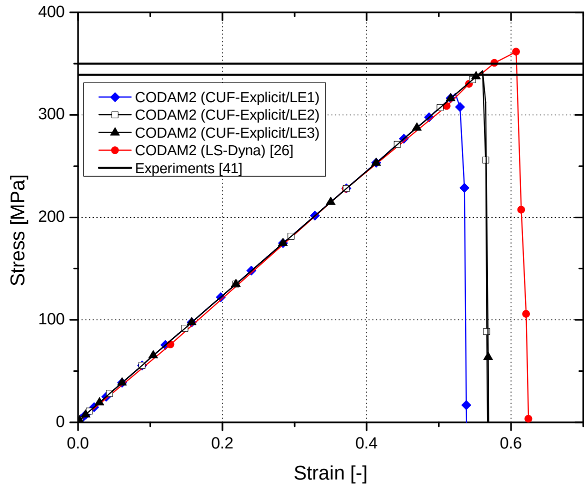

Figure 5: Stress-strain curve for the scale-8 centre-notched tension specimen with $[45/90/-45/0]_{4s}$ layup

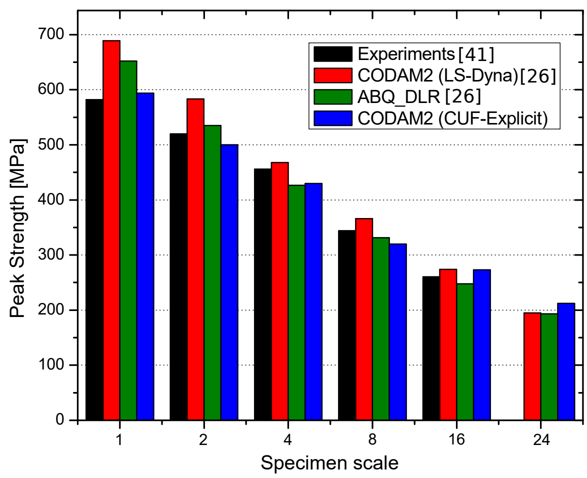

Figure 6: Comparison of the peak strength obtained by various numerical approaches and experimental measurements for the centre-notched tensile specimens with $[45/90/-45/0]_{4s}$ layup. The influence of specimen size on the peak strength of the specimen is clearly observed.

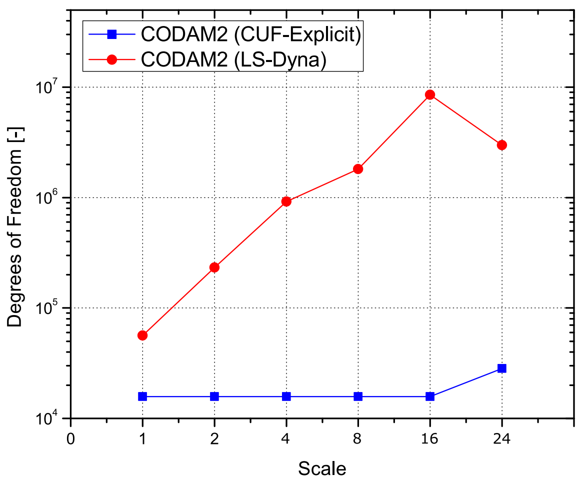

(a) Degrees of Freedom

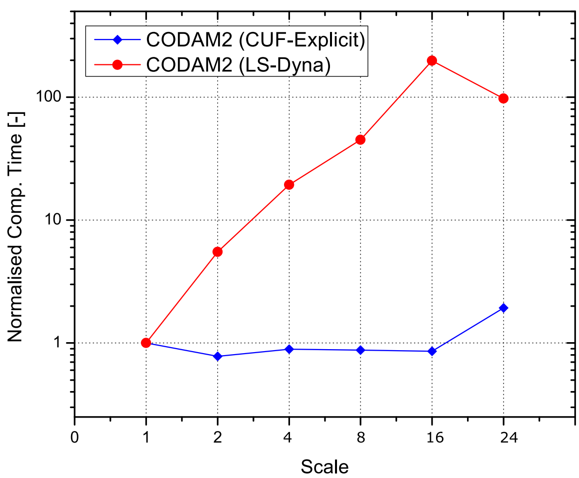

(b) Normalised Computational Time

Figure 7: Degrees of freedom and normalised computational time required for the numerical analysis of the various CNT scales in CUF-Explicit and LS-DYNA

4. The scale-24 analysis (for a fictitious large scale structure where no experimental results are available) is performed using a coarser mesh density in LS-DYNA, resulting in a reduction of the computational effort. The CUF model requires a finer mesh compared to the other scales, but nevertheless maintains significant computational efficiency compared to LS-DYNA.

4.3 Over-height compact tension test of dispersed-ply laminate

The last numerical assessment considers an over-height compact tension specimen with a dispersed ply sequence of $[90/45/0/-45]_{4s}$, resulting in a quasi-isotropic laminate. The OCT loading geometry results in a stable crack growth, while the use of a dispersed ply sequence makes the laminate less prone to delamination. A schematic representation of the OCT with dimensions and applied boundary conditions is given in Fig. 8. A gradually increasing displacement u (up to 1.0 mm) is prescribed on each pin in opposite directions, leading to a pin opening displacement (POD) of $2u$. The CUF-Explicit analysis uses a mesh consisting of 392 quadratic (Q9) elements within the plane, and three models are considered with linear (LE1), quadratic (LE2) and cubic (LE3) ply thickness expansions, respectively. Reference numerical results are obtained from [26], while experimental data is available in [42].

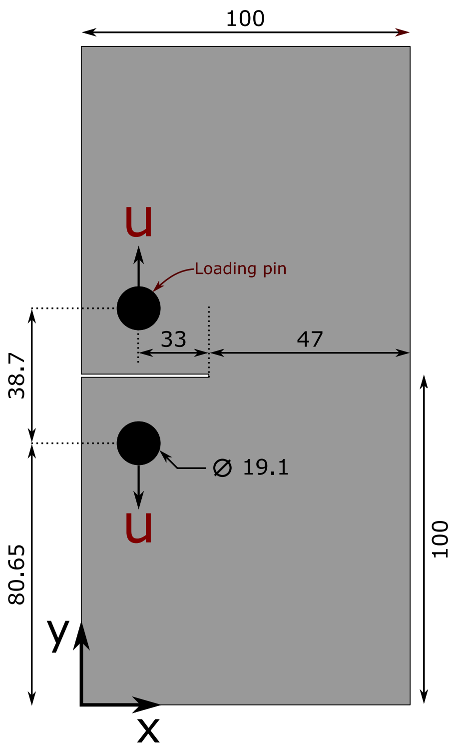

Figure 8: Schematic representation of the over-height compact tensile specimen with a $[90/45/0/-45]_{4s}$ quasi-isotropic dispersed ply sequence along with loading conditions (dimensions in mm)

The predicted and measured load-displacement response of the laminate are overlaid in Fig. 9. The evolution of the crack length as a function of the POD has been plotted in Fig. 10. The crack length is determined by considering the extent of fibre damage saturation in the 0° ply of the laminate, where damage is considered to be saturated when the fibre damage parameter, defined in Eq. 24, reaches a value of unity ($\omega_1 = 1.0$). The contour plot of fibre and matrix damage in the 0° and 90° plies, respectively, is shown in Fig. 11, for a POD of 1.5 mm.

The following observations are made

1. From Fig. 9, it is seen that the peak force obtained with the LE1 model matches that reported by the reference LS-DYNA solution, while the LE3 model predicts a slightly higher peak force. The post-peak softening curve in both cases is in good general agreement with the experimental curve.

2. The differences between the LS-DYNA and the CUF-Explicit solutions, in the linear regime, stems from the structural theories used in the models. The LS-DYNA model is developed using stacked thick shell elements, while the CUF-Explicit model uses a combination of quadratic (Q9) elements within the plane and Lagrange polynomial expansions of varying order through the thickness for each ply of the laminate.

3. A non-negligible amount of numerical oscillations can be observed in the softening curve of the CUF-Explicit models. This stems from the use of a fully-integrated second-order (Q9) in-plane mesh, and the absence of numerical damping.

4. The crack length evolution shown in Fig. 10 is in good agreement with experimental data, however with a delayed damage initiation. The same delayed response is also observed in the force-displacement curve in Fig. 9.

5 Discussion

The initial numerical assessments based on single element tests show the characteristics of the CODAM2 damage model. Tensile loading under uni-axial strain conditions, along and transverse to the fibre direction, results in a bilinear stress-strain behaviour as seen in Fig. 2. Under loading in the fibre direction, the peak stress coincides with the fibre strength X_T following which the load carrying capacity reduces linearly until the damage saturation strain is reached. A similar bilinear behaviour holds for transverse loading where damage occurs in the matrix, with an associated matrix fracture energy $G_2^f = 2.6\ kJ/m^2$. The peak stress under transverse loading corresponds to the matrix strength Y_T. Furthermore, the area under the curves of Fig. 2a and Fig. 2b are consistent with the input value of the fracture energy for the fibre and matrix, respectively. The stress-strain response of the single element laminate is in good agreement with the reference CODAM2 implementation in LS-DYNA, as seen in Fig. 3. The variation between the two numerical approaches prior to final failure is attributed to the fact that the present work does not consider in-plane shear non-linearity, while it is present in the LS-DYNA implementation.

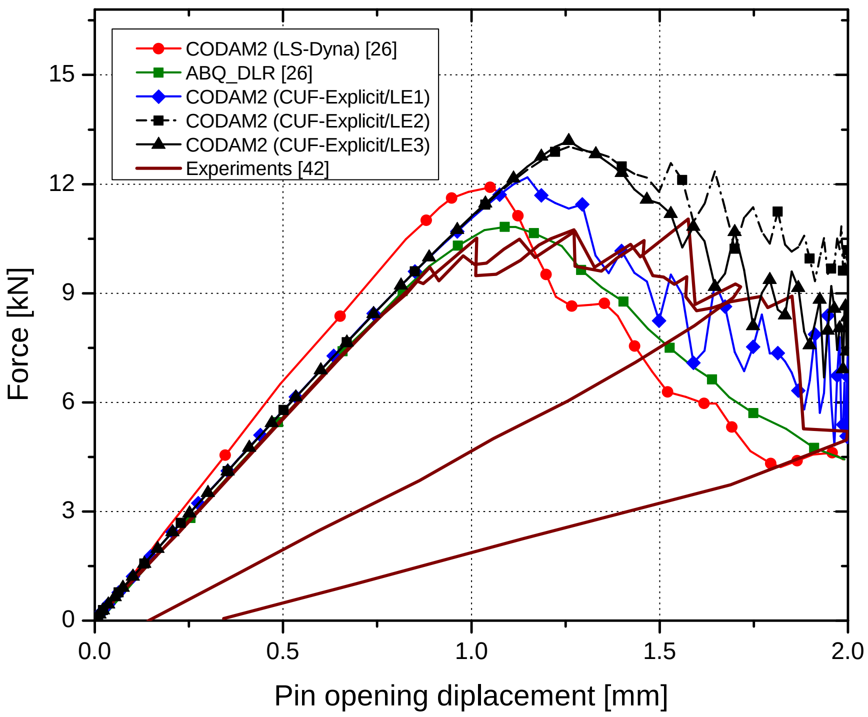

Figure 9: POD-Force curve for the OCT test of dispersed $[90/45/0/-45]_{4s}$ IM7/8552 CFRP laminates

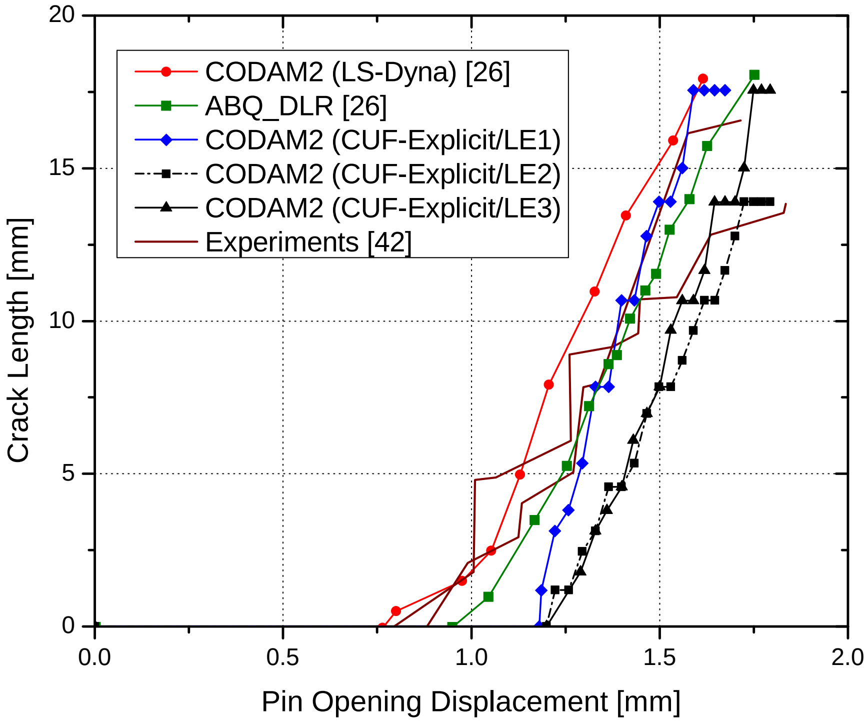

Figure 10: Crack length evolution in the 0° ply for the OCT test of dispersed $[90/45/0/-45]_{4s}$ IM7/8552 CFRP laminates

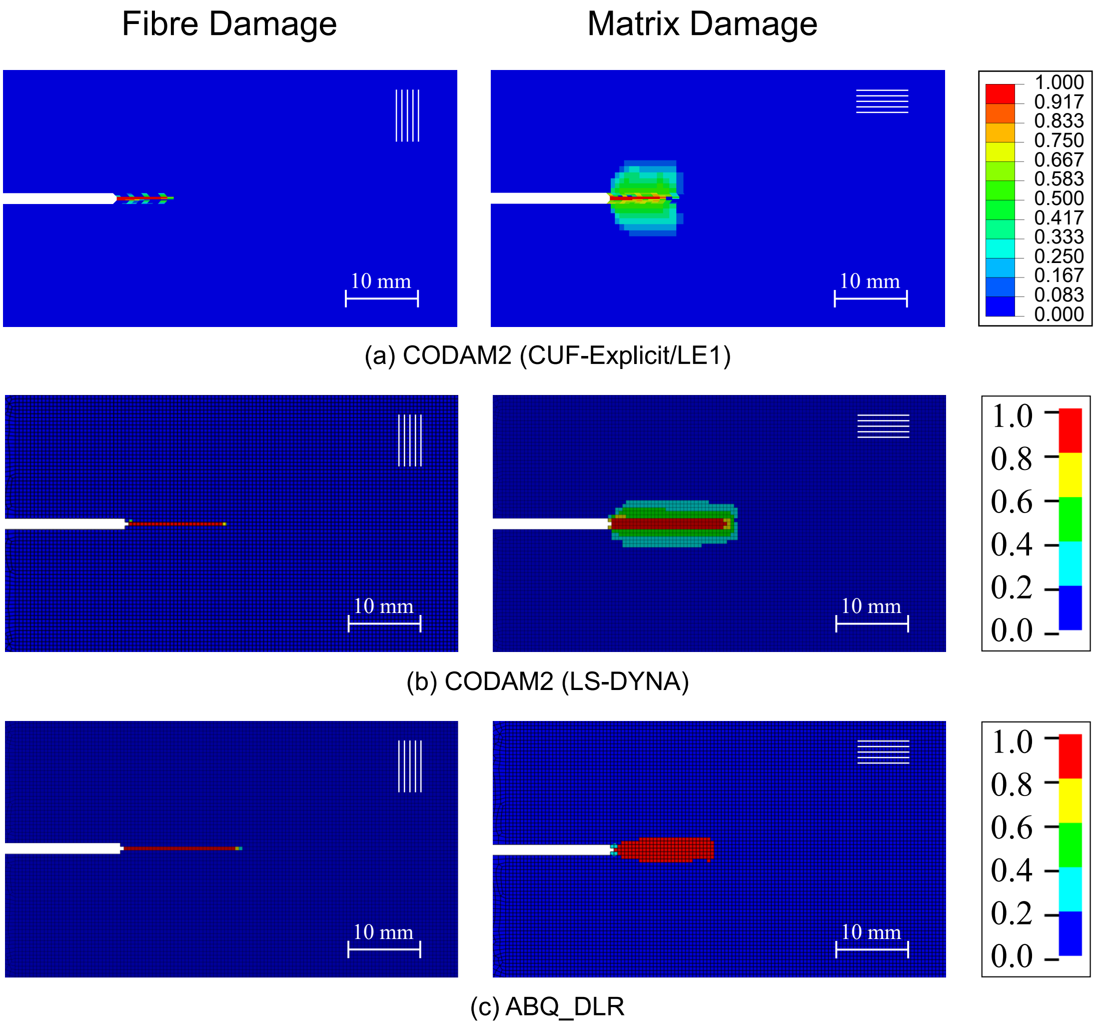

Figure 11: Distribution of the fibre damage in the 0° ply (left) and matrix damage in the 90° ply (right) near the notch for the $[90/45/0/-45]_{4s}$ IM7/8552 CFRP quasi-isotropic laminate, at a POD of 1.5 mm. (a) CODAM2 (CUF-Explicit/LE1), (b) CODAM2 (LS-DYNA) [26], and (c) *ABQ_DLR* [26].

The use of higher-order finite elements in the continuum damage modelling of composite laminates using explicit codes is largely unexplored in the literature, where the standard approach is to use linear solid elements with reduced integration. Conversely, the present work uses CUF-based higher-order structural models, which can offer several advantages in the progressive damage analysis of composites. The use of expansion functions to enrich the through-thickness kinematics of individual plies results in an accurate resolution of interlaminar stress fields, which are critical inputs to damage models, especially in the case of delamination. The influence of expansion order through the thickness is seen in Fig. 5, where the use of second-order LE2 functions show an improvement in peak stress predictions over the first-order LE1 expansion, keeping the in-plane discretisation constant. Increasing the expansion order further does not lead to any significant effects, since in-plane loading is considered, and delamination is not taken into account. Another characteristic of CUF structural theories is the weak dependency between the size of the structure and the mesh, which is in strong contrast to standard FEA. This is seen in Fig. 6, where the discretisation is kept constant for scales 1-16 of the centre-notched tensile specimen, without affecting the accuracy of the result. Such an approach results in a constant DOF value as seen in Fig. 7a, and consequently, the computational time required also remains fairly constant, as seen in Fig. 7b. On the other hand, an exponential increase in both DOF and computational times can be observed for the case of standard FEA. These aspects could have significant advantages in improving the computational efficiency during the progressive damage analysis of large-scale composite structures.

The final assessment is the simulation of progressive damage in dispersed $[90/45/0/-45]_{4s}$ over-height compact tension (OCT) quasi-isotropic laminates, described in Section 4.3. The predictions of the current framework are in good general agreement with reference numerical and experimental data, as seen in Fig. 9 and Fig. 10, which show the global force-displacement response and the crack-length evolution, respectively. The LE3 model predicts a higher peak force compared to the LE1 and the reference LS-DYNA results, but exhibits a good correlation with experimental data in the regime of progressive damage. The predictive capability of the numerical framework can be further improved by a combination of higher-order thickness expansion functions and physically accurate shear behaviour, i.e., considering nonlinear shear effects. A consequence of using higher-order models is the presence of numerical oscillations. This is clearly observed in Fig. 9, where the post peak softening curve shows an oscillatory response. These spurious oscillations can stem from the fact that fully-integrated higher-order elements are used in the present approach, which can cause excitation of the highest frequency components. The use of different integration schemes, for instance reduced-integration, and damping techniques such as bulk viscosity damping, are possible strategies to mitigate such numerical oscillations, and is an area for future investigation.

6 Conclusion

The current work presents the development of an explicit transient dynamics framework for the progressive tensile damage analysis of composite structures. The ply-level CODAM2 intralaminar damage model, with stress-based failure initiation criteria, has been used to describe the damage behaviour of the composite material, while higher-order structural theories based on the Carrera Unified Formulation are used for the layer-wise structural modelling of the composite laminate. Several validation cases have been considered for the proposed framework, based on the IM7/8552 carbon fibre reinforced polymer material system, and the results have been compared with experimental data as well as reference numerical predictions using LS-DYNA and ABAQUS.

The initial verification of the damage model implementation was demonstrated via a series of single element tests. Coupon-level assessments were then performed on centre-notched tensile laminated specimens with quasi-isotropic layup, over a range of specimen sizes. The final validation case was the over-height compact tension test of quasi-isotropic dispersed laminates. The predictions of the proposed framework were in good general agreement with reference numerical and experimental results. In the case of centre-notched quasi-isotropic dispersed laminates, size-effects were predicted with reasonable accuracy. The advantages of CUF-based higher-order structural models was discussed, in particular the savings in computational costs and the capability to tailor structural models by increasing the order of the thickness expansion functions, according to the requirements of the analysis. These advantages of the proposed framework could thus potentially make it a suitable candidate for the computationally-efficient progressive damage analysis of composite structures.

Future investigations include extending the present work to compressive damage, and the inclusion of cohesive zone modelling to account for delamination. A suitable application for the resulting framework would be low-velocity impact analysis of composite structures.

Acknowledgements

This research work has been carried out within the project ICONIC (Improving the Crashworthiness of Composite Transportation Structures), funded by the European Union Horizon 2020 Research and Innovation program under the Marie Skłodowska-Curie Grant agreement No. 721256, and the Joint Project for the Internationalization of Research // Polito MUL2 — University of British Columbia. Computational resources were provided by HPC @ POLITO (http://www.hpc.polito.it).

References

[1] A. C. Orifici, I. Herszberg, and R. S. Thomson. Review of methodologies for composite material modelling incorporating failure. *Composite structures*, 86(1-3):194–210, 2008.

[2] J. Reiner and R. Vaziri. Structural analysis of composites with finite element codes: An overview of commonly used computational methods. In P.W.R. Beaumont and C.H. Zweben, editors, *Comprehensive Composite Materials II*, volume 8, pages 61–84. Oxford: Academic Press, 2018.

[3] M. F. S. F de Moura and J. P. M. Gonçalves. Modelling the interaction between matrix cracking and delamination in carbon–epoxy laminates under low velocity impact. *Composites Science and Technology*, 64(7-8):1021–1027, 2004.

[4] S. R. Hallett, W. Jiang, B. Khan, and M. R. Wisnom. Modelling the interaction between matrix cracks and delamination damage in scaled quasi-isotropic specimens. *Composites Science and Technology*, 68(1):80–89, 2008.

[5] C. Bouvet, B. Castanié, M. Bizeul, and J. Barrau. Low velocity impact modelling in laminate composite panels with discrete interface elements. *International Journal of Solids and Structures*, 46(14-15):2809–2821, 2009.

[6] X. C. Sun, M. R. Wisnom, and S. R. Hallett. Interaction of inter-and intralaminar damage in scaled quasi-static indentation tests: Part 2–numerical simulation. *Composite Structures*, 136:727–742, 2016.

[7] J. Reiner, M. Veidt, M. Dargusch, and L. Gross. A progressive analysis of matrix cracking-induced delamination in composite laminates using an advanced phantom node method. *Journal of Composite Materials*, 51(20):2933–2947, 2017.

[8] M. J. Swindeman, E. V. Iarve, R. A. Brockman, D. H. Mollenhauer, and S. R. Hallett. Strength prediction in open hole composite laminates by using discrete damage modeling. *AIAA journal*, 51(4):936–945, 2013.

[9] H. W. Wang, H. W. Zhou, H. W. Ji, and X. C. Zhang. Application of extended finite element method in damage progress simulation of fiber reinforced composites. *Materials & Design*, 55:191–196, 2014.

[10] B. Y. Chen, S. T. Pinho, N. V. de Carvalho, P. M. Baiz, and T. E. Tay. A floating node method for the modelling of discontinuities in composites. *Engineering Fracture Mechanics*, 127:104–134, 2014.

[11] J. Reiner. A computational investigation of failure modes in hybrid titanium composite laminates. 2016.

[12] Z. P. Bažant and B. H. Oh. Crack band theory for fracture of concrete. *Matériaux et construction*, 16(3):155–177, 1983.

[13] P. Ladeveze and E. LeDantec. Damage modelling of the elementary ply for laminated composites. *Composites science and technology*, 43(3):257–267, 1992.

[14] A. Matzenmiller, J. Lubliner, and R. L. Taylor. A constitutive model for anisotropic damage in fiber-composites. *Mechanics of materials*, 20(2):125–152, 1995.

[15] P. P. Camanho, P. Maimí, and C. G. Dávila. Prediction of size effects in notched laminates using continuum damage mechanics. *Composites science and technology*, 67(13):2715–2727, 2007.

[16] E. Kim, M. Rim, I. Lee, and T. Hwang. Composite damage model based on continuum damage mechanics and low velocity impact analysis of composite plates. *Composite Structures*, 95:123–134, 2013.

[17] L. Wang, C. Zheng, H. Luo, S. Wei, and Z. Wei. Continuum damage modeling and progressive failure analysis of carbon fiber/epoxy composite pressure vessel. *Composite Structures*, 134:475–482, 2015.

[18] K. Song, Y. Li, and C. Rose. Continuum damage mechanics models for the analysis of progressive failure in open-hole tension laminates. In *52nd AIAA/ASME/ASCE/AHS/ASC Structures, Structural Dynamics and Materials Conference 19th AIAA/ASME/AHS Adaptive Structures Conference*, page 1861, 2011.

[19] R. M. Frizzell, C. T. McCarthy, and M. A. McCarthy. Simulating damage and delamination in fibre metal laminate joints using a three-dimensional damage model with cohesive elements and damage regularisation. *Composites Science and Technology*, 71(9):1225–1235, 2011.

[20] D. Feng and F. Aymerich. Finite element modelling of damage induced by low-velocity impact on composite laminates. *Composite Structures*, 108:161–171, 2014.

[21] A. Forghani and R. Vaziri. Computational modeling of damage development in composite laminates subjected to transverse dynamic loading. *Journal of Applied Mechanics*, 76(5):051304, 2009.

[22] K. V. Williams, R. Vaziri, and A. Poursartip. A physically based continuum damage mechanics model for thin laminated composite structures. *International Journal of Solids and Structures*, 40(9):2267–2300, 2003.

[23] C. McGregor, N. Zobeiry, R. Vaziri, A. Poursartip, and X. Xiao. Calibration and validation of a continuum damage mechanics model in aid of axial crush simulation of braided composite tubes. *Composites Part A: Applied Science and Manufacturing*, 95:208–219, 2017.

[24] S. Ofir and R. Vaziri. Application of the local cohesive zone method to numerical simulation of composite structures under impact loading. *International Journal of Impact Engineering*, 104:127–149, 2017.

[25] A. Forghani, N. Zobeiry, A. Poursartip, and R. Vaziri. A structural modelling framework for prediction of damage development and failure of composite laminates. *Journal of Composite Materials*, 47(20-21):2553–2573, 2013.

[26] J. Reiner, T. Feser, D. Schueler, M. Waimer, and R. Vaziri. Comparison of two progressive damage models for studying the notched behavior of composite laminates under tension. *Composite Structures*, 207:385–396, 2019.

[27] A. Forghani, A. Poursartip, and R. Vaziri. An orthotropic non-local approach to modeling intra-laminar damage progression in laminated composites. *International Journal of Solids and Structures*, 180:160–175, 2019.

[28] M. Shahbazi. *An efficient virtual testing framework to simulate the progression of damage in notched composite laminates.* PhD thesis, University of British Columbia, 2017.

[29] E. Carrera, M. Cinefra, M. Petrolo, and E. Zappino. *Finite element analysis of structures through unified formulation.* John Wiley & Sons, 2014.

[30] A. Pagani and E. Carrera. Unified formulation of geometrically nonlinear refined beam theories. *Mechanics of Advanced Materials and Structures*, 25(1):15–31, 2018.

[31] M. Petrolo, M. H. Nagaraj, I. Kaleel, and E. Carrera. A global-local approach for the elastoplastic analysis of compact and thin-walled structures via refined models. *Computers & Structures*, 206:54–65, 2018.

[32] I. Kaleel, M. Petrolo, A. M. Waas, and E. Carrera. Micromechanical progressive failure analysis of fiber-reinforced composite using refined beam models. *Journal of Applied Mechanics*, 85(2):021004, 2018.

[33] I. Kaleel, M. Petrolo, E. Carrera, and A. M. Waas. Computationally efficient concurrent multiscale framework for the linear analysis of composite structures. *AIAA Journal*, 57(9):4019–4028, 2019.

[34] I. Kaleel, M. Petrolo, E. Carrera, and A. M. Waas. Computationally efficient concurrent multiscale framework for the nonlinear analysis of composite structures. *AIAA Journal*, 57(9):4029–4041, 2019.

[35] E. Carrera and M. Petrolo. Refined beam elements with only displacement variables and plate/shell capabilities. *Meccanica*, 47(3):537–556, 2012.

[36] E. Zappino, G. Li, A. Pagani, and E. Carrera. Global-local analysis of laminated plates by node-dependent kinematic finite elements with variable esl/lw capabilities. *Composite Structures*, 172:1–14, 2017.

[37] R. de Borst, M. A. Crisfield, J. J. C. Remmers, and C. V. Verhoosel. *Nonlinear finite element analysis of solids and structures.* John Wiley & Sons, 2012.

[38] Z. Hashin. Failure criteria for unidirectional fiber composites. *Journal of applied mechanics*, 47(2):329–334, 1980.

[39] A. S. Kaddour, M. J. Hinton, P. A. Smith, and S. Li. Mechanical properties and details of composite laminates for the test cases used in the third world-wide failure exercise. *Journal of Composite Materials*, 47(20-21):2427–2442, 2013.

[40] J. Reiner, N. Zobeiry, R. Vaziri, T. Feser, M. Waimer, D. Schueler, and N. Toso-Pentecôte. Prediction of damage progression in notched tensile specimens: comparison between two intralaminar damage models. In

VI ECCOMAS Thematic Conference on the Mechanical Response of Composites. Eindhoven, Netherlands, 2017.

[41] X. Xu, M. R. Wisnom, X. Li, and S. R. Hallett. A numerical investigation into size effects in centre-notched quasi-isotropic carbon/epoxy laminates. *Composites Science and Technology*, 111:32–39, 2015.

[42] N. Zobeiry, R. Vaziri, and A. Poursartip. Characterization of strain-softening behavior and failure mechanisms of composites under tension and compression. *Composites Part A: Applied Science and Manufacturing*, 68:29–41, 2015.